Emergence of Deep Traps in Long-Term Thermally Stressed $CH_3NH_3PbI_3$ Perovskite Revealed by Thermally Stimulated Current

Motiur R. Khan[1], Jonas A. Schwenzer[1], Jonathan Lehr[1], Ulrich W. Paetzold*[1,2] and Uli Lemmer*[1,2]*

[1] Light Technology Institute, Karlsruhe Institute of Technology, Engesserstrasse 13, 76131 Karlsruhe, Germany

[2] Institute of Microstructure Technology, Karlsruhe Institute of Technology, Hermann-von Helmholtz-Platz 1, 76344 Eggenstein-Leopoldshafen, Germany

Corresponding Authors

*Motiur R. Khan (motiur.khan@kit.edu)

*Ulrich W. Paetzold (ulrich.paetzold@kit.edu)

*Uli Lemmer (ulrich.lemmer@kit.edu)

Abstract: Defect states are known to trigger trap-assisted non-radiative recombination, restricting the performance of perovskite solar cells (PSCs). Here, we investigate the trap states in long-term thermally stressed methylammonium lead iodide ($MAPbI_3$) perovskite thin films over 500 hours at 85 ^oC employing thermally stimulated current measurements. A prominent deep trap level was detected with activation energy ~ 0.459 eV in $MAPbI_3$ without thermally stressed. Interestingly, upon the thermal stress, an additional deep trap level of activation energy ~ 0.414 eV emerges and grows with thermal stress duration. After 500 hours of thermal stress, trap density was ~ 10^{16} cm^{-3}. The trend of open-circuit voltage loss was in line with the trap density variation with thermal stress time, which elucidates the enhanced non-radiative recombination through these trap states. This work opens a path to understanding the mechanism behind long-term thermal instability and further inspires developing strategies to minimize trap formation in PSCs.

Keywords: traps, thermally stimulated current, thermal stress, perovskite solar cells, long-term stability, thermal degradation

TOC Graphic

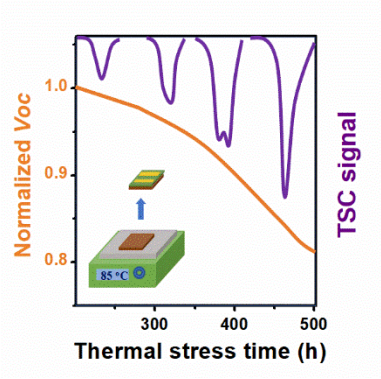

Strive for developing high-performance power conversion efficiency (PCE) of hybrid organic-inorganic perovskite solar cells has brought them to the forefront in the thin film photovoltaics technologies reaching 25.5 % in a short period of time.[1–3] Along this line, the development in compositional engineering and a variety of solution processing methods for high-quality perovskite film fabrication have played a significant role.[4–9] Despite the tremendous growth in PCEs, several key issues related to recombination loss, long-term stability, and up-scaling to large-area devices are the main obstacles in the commercialization of perovskite solar cells and need to be tackled. [10–16] It has been realized that defect states acting as charge carrier recombination centers constitute a major recombination loss, hamper electronic transport, and further induce the stability even of high-performance devices.[17–21] Therefore, it is of immense importance to obtain more information on the parameters of traps such as activation energy, trap density, their origin, and finally, their effect on solar cell performances and stability.

The formation of defect states is closely related to the morphology of the perovskite thin film, which strongly depends on the precursor materials, the processing methods, and the external conditions during preparation. Shi et al. have observed exceptionally low trap densities in the order of 10^9-10^{10} cm^{-3} in $MAPbI_3$ single crystals processed via the antisolvent vapor-assisted crystallization approach while solution-processed $MAPbI_3$ shows higher trap densities (~10^{17} cm^{-3}).[22] In principle, there are different possibilities of defects in perovskite crystals, e.g., vacancies, interstitials, and substitutions, as also indicated by density functional theory (DFT) calculations.[23–27] However, their formation energies also depend on the fabrication conditions and the environment.[28–31] The intrinsic point defect of iodine, I_{Pb} (I atoms at Pb sites) with activation energy ~ 0.6eV was reported as the dominant defect in $MAPbI_3$ processed from the one-step spin-coating method, while I_{MA} (I atoms at MA sites) defect with activation energy ~ 0.75 eV was the dominant one in $MAPbI_3$ films deposited via the two-step process.[32] The authors used deep-level transient spectroscopy to probe these trap states. Moreover, a deep trap of energy ~ 0.5 eV with trap concentration ~ 10^{16} cm^{-3} was observed in a two-step processed $MAPbI_3$ film.[33] It was recently demonstrated that the inclusion of formamidinium leads to suppression of the defect states in $MAPbI_3$ thin films.[34]

Apart from intrinsic defect formation during crystallization of perovskites under various conditions, they are prone to form the defect states under real working conditions. The formation of defect states has been shown to be

induced by continuous light illumination, oxygen, and moisture in $MAPbI_3$ perovskite.[35–38] The effect of the electric field has been shown to induce the ion migration introducing the defect states on the continuous working condition of the cell.[21,39]

The effect of long-term thermal stress on $MAPbI_3$ has been widely reported in terms of its decomposition and the consequence on solar cell performance. Temperature-dependent stability of $MAPbI_3$ was reported, and kinetics of perovskite degradation at elevated temperatures (at 85 ^oC) for a longer period of time (750 h) was established.[40] In other reports, the thermal decomposition of $MAPbI_3$ was observed in different environmental conditions.[41,42] Our group showed the outdoor temperature variation effect on the degradation and, hence, $MAPbI_3$ solar cells' performance.[20,43] However, reports on the impact of long-term thermal stress in terms of trap states formation and their correlation with solar cell performance are lacking.

Here, we systematically probe the trap states in $MAPbI_3$ by varying the thermal stress time using the thermally stimulated current (TSC) technique. TSC is a highly sensitive method to estimate the trap density and activation energy of traps in semiconductor materials.[44–46] TSC measurements directly correlate the observed trap states to the device performance as it is performed on fully working solar cells. It has been successfully applied to probe the suppression of traps by incorporating Cs in a multiple-cation mixed-halide, leading to enhanced solar cell performance.[47] A large density of trap formation in perovskite solar cells (PSCs) after degradation by continuous solar illumination for 500 h was observed using the TSC technique.[35] Most of the TSC reports on PSCs are limited to comparative measurements on reference and modified samples.[37,48] Here, we present TSC studies on a series of long-term thermally stressed $MAPbI_3$ PSCs and the evolution of the trap density as a function of thermal stress duration extending up to 500 h at 85 ^oC. We show the formation of deep trap states in perovskite upon thermal stress. We find an enhancement in the density of traps with increasing the thermal stress time which correlates to the trend in open-circuit voltage loss, likely due to the trap-assisted carrier recombination in the perovskite. Although perovskite solar cells have reached 25.5 % efficiency, long-term thermal instability at elevated temperatures remains a bottleneck for their industrialization. The detrimental effect of the environmental factors such as moisture, oxygen, etc., on the long-term stability can be minimized by proper sealing of the cells,

but the elevated temperature effect due to the direct sun still remains an inevitable issue for the stability of the perovskite solar cells. Our work will contribute significantly to understanding the effect of long-term thermal stress on the thermal stability of perovskite solar cells, which encourages further studies on the perovskite solar cells with high power conversion efficiencies.

For the TSC measurement, the device is cooled down to a low temperature in the dark, well below the activation energies of the traps, and then charge carriers are generated by white LED illumination. Once the illumination is switched off, the generated charge carriers relax and occupy the available trap states during the thermalization process. The trapped carriers are gradually released as they gain enough thermal energy to escape by increasing the device temperature at a constant ramp rate (7 K/min in our experiments). These de-trapped carriers are simultaneously monitored in the form of current as a function of temperature, commonly known as a TSC spectrum used to determine the activation energy of trap states and the corresponding trap density.

We studied the $MAPbI_3$ perovskite solar cells with the device structure indium tin oxide (ITO)/tin oxide (SnO_2)/ $MAPbI_3$/2,2′,7,7′-tetrakis[*N*,*N*-di(4-methoxyphenyl)amino]-9,9′-spirobifluorene (spiro-MeOTAD)/Au. Thermal stress at elevated temperatures could create degradation in perovskite as well as in charge transport layers. There is a possibility of interface modification between spiro-MeOTAD and perovskite at elevated temperatures. Therefore, thermal treatment of $MAPbI_3$ perovskite was performed before the deposition of spiro-MeOTAD and investigation of the effect of thermal stress on the perovskite only was done by thermally exposing $MAPbI_3$ films on SnO_2 in the dark under an inert atmosphere for different time intervals. In this way, we narrowed down the origin of degradation.

The current density versus voltage (*J*-*V*) characteristics of all the solar cells, pristine and thermally treated, were evaluated under one sun illumination, as shown in Figure 1a.

The overall performances of the solar cells reduce with increased duration of thermal stress. The reduction in solar cell performance can be attributed to the significant decrease in all the solar cell parameters (Figure 1b). The initial decay in the fill factor (FF) and short-circuit current density (*J*sc) is comparatively slower than the fall in

open-circuit voltage (*V*oc). The *V*oc is found to reduce continuously with increasing the thermal stress time up to 500 h.

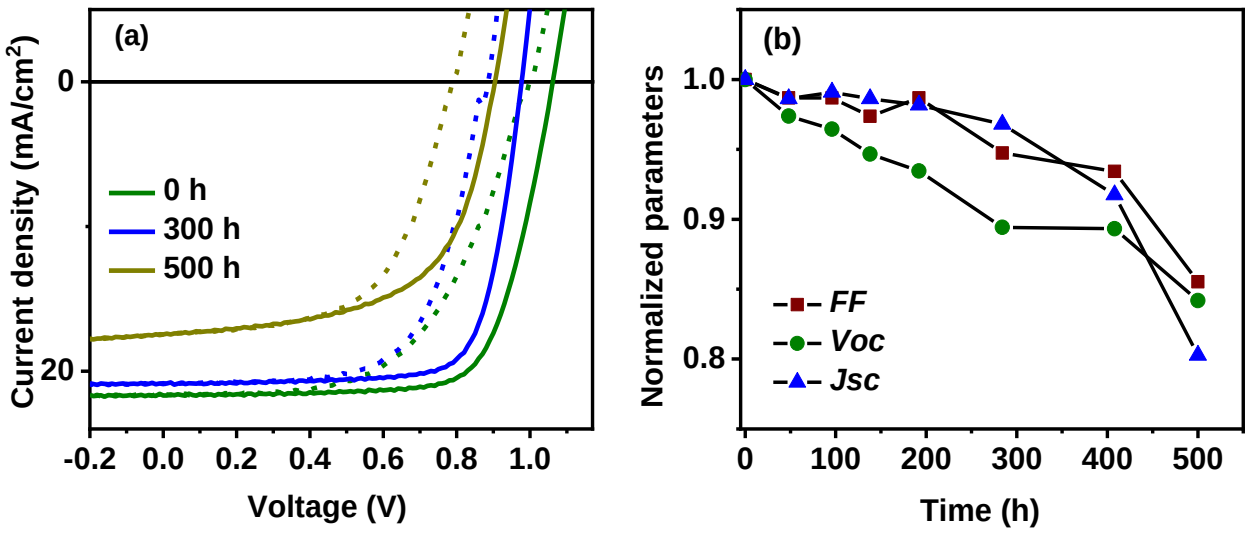

Figure 1. (a) *J-V* characteristics of the $MAPbI_3$ devices with forward (dashed line) and backward (solid line) bias scan fabricated without thermal treatment and after different thermal treatment time at 85 °C under a solar simulator with irradiance of 100 mW/cm^2 optical power (b) Solar cell parameters (*Voc*, FF, *Jsc*) from backward *J-V* scan with thermal treatment time for $MAPbI_3$ solar cells normalized to the values of the pristine sample.

The different reduction trends in the different solar cell parameters with thermal treatment time indicate that separate mechanisms are responsible for *J*sc, FF, and *V*oc reduction. The plausible reasons for the decrease in each parameter and their trends are discussed elsewhere.[49] Here, our focus is on investigating trap states in PSCs thermally stressed for different interval of times using the TSC method and establishing a correlation with *V*oc reduction as the trap states have a direct consequence on *V*oc.

Figure 2 shows the TSC signals as a function of temperature for the pristine device with no thermal stress and thermally stressed devices for 300, 400, and 500 hours. In the pristine device, three distinct peaks were observed at temperatures around 110 K, 171 K, and 225 K (denoted as P1, P2, and P3, respectively), indicating the

distribution of three different trap levels. To check the heat cycle effect during the measurement on the degradation of the perovskite sample, we performed two consecutive TSC measurements resulting in quite similar spectra (see Figure S1). This confirms that the heat cycle between 15 K and room temperature does not degrade the perovskite. The dominant effect of the thermal stress was the emergence of a new peak shoulder at around 205 K (denoted as P4) for the device stressed for 300 hours which becomes more distinct for the device stressed for 400 hours.

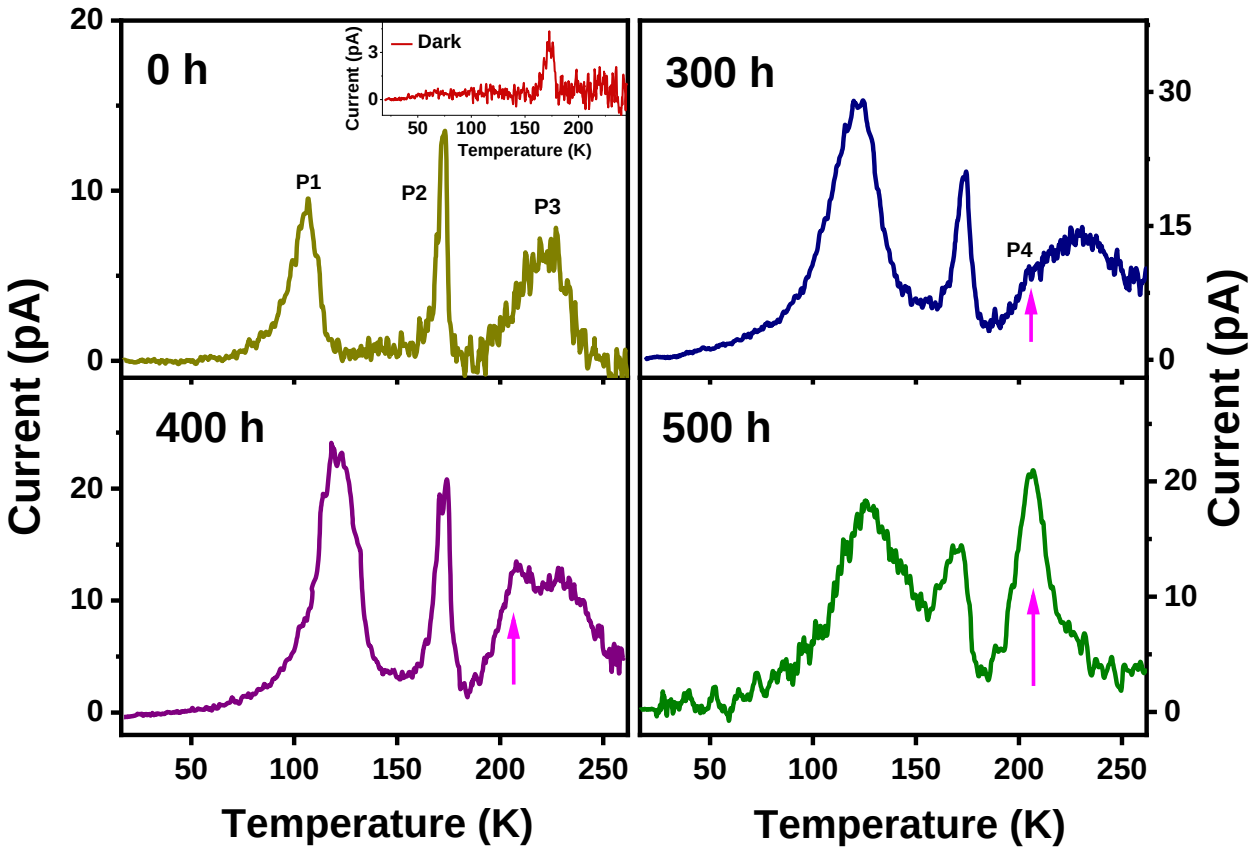

Figure 2. TSC spectra of $MAPbI_3$ solar cells without thermal treatment and for the samples that were thermally stressed for 300, 400, and 500 hours before the HTL deposition. Inset shows the TSC spectrum without illuminating the sample. The arrow indicates the emergence of a new peak (P4) in thermally stressed $MAPbI_3$.

Finally, for the device with the most extended period of thermal stress (500 hours), the new peak emerged as a complete profile dominating over the peak at around 225 K. As these TSC peaks could originate from the perovskite as well as from the transport layers, we have performed control experiments on the devices with and without transport layers. Unfortunately, $MAPbI_3$ without transport layers exhibited too high leakage current. We, therefore, decided to perform control experiments using multication formamidinium cesium lead iodide (FACs)) with and without transport layers as shown in Figure 3. Two TSC peaks were observed in the device with transport layers at ~ 110 K and ~ 225 K.

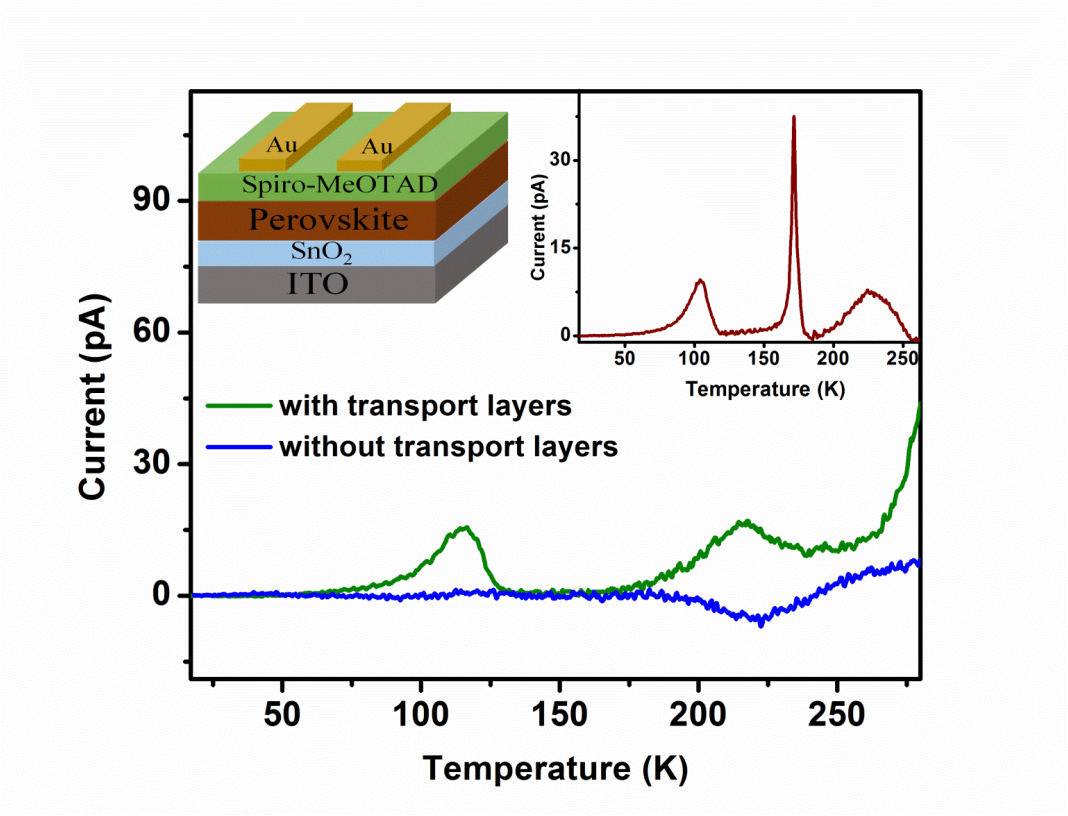

Figure 3**.** TSC spectra of multication (FACs) perovskite solar cells with and without the transport layers. Inset shows the TSC spectrum of pristine $MAPbI_3$ with TiO_2 as ETL and spiro-MeOTAD as HTL.

However, in the device without transport layers, low temperature peak disappeared, and only the higher temperature peak at ~ 225 K was observed. For the device without transport layers, the sign of the TSC signal is reversed. This finding is in agreement with the previous report and is attributed to a reversal of the sign of the

built-in electric field.[33] The disappearance of the TSC peak at ~ 110 K confirms its origin in one of the transport layers. To further narrow down the source of P1, we performed TSC measurements by replacing SnO_2 electron transport layer (ETL) with TiO_2 in TiO_2/$MAPbI_3$/ spiro-OMeTAD device geometry with pristine perovskite resulting in very similar peaks as P1, P2 and P3, which shows that P1 does not belong to the ETL or ETL/perovskite interface. We further compared the current results with our previous TSC work on triple cation and multication perovskite with electron layers as TiO_2 and SnO_2, respectively, with the common hole transport layer spiro-OMeTAD. TSC studies on both the device structures exhibit a similar peak as P1, which suggests its origin in spiro-OMeTAD layer.[48,50] There could be a possibility of interface traps between hole transport layer and perovskite which could eventually give rise to a TSC signal. However, recent studies on MAPI using TSC measurements with various hole transport layers do not support this notion and the origin of traps was found to be in the bulk of perovskite.[33,51] Thus, we assign the low-temperature peak (at ~ 110 K) in Figure 2 to the spiro-OMeTAD layer while the remaining peaks are assigned to the $MAPbI_3$ layer. The peak P2 (at ~ 170 K) was observed in all the devices. However, it should be noted that the peak P2 appeared even in the dark TSC scan without filling the traps as well (inset of Figure 2). Similar behavior was observed by Baumann et al. in $MAPbI_3$ film at ~ 163 K, where they have assigned such phenomena to a phase transition occurring around this temperature from orthorhombic to tetragonal, creating a displacement current by a movement of the ions during phase transition.[28,33] We, therefore, focus on the peaks appearing at temperatures above the phase transition temperature as these are relevant to the device performance. It is to be noted that the polarity of the traps, whether electron or hole traps, is not known due to the complete solar cell configuration of the device, and the photo-generated carriers can fill the electron as well as hole traps. The average activation energy corresponding to peak P3, which is intrinsically present in the pristine device, can be calculated using equation [52]

$$E_t = k_B T_m ln\,(T_m^4/\beta)$$

where k_B is the Boltzmann's constant, T_m is the temperature at the TSC peak, and β is the heating rate (7 K /min). The above relation was obtained with the assumption of a temperature-dependent effective density of states $N(T)$ of the respective band and a temperature-dependent thermal velocity of the carriers $v(T)$ by Fang et al. However, assumption of temperature-independent N and v results in a different relation as shown by Bube (See Supporting

Information (SI) for more details).[53] For a pristine device without thermal treatment, the average trap activation energy corresponding to P3 is found to be ~ 0.459 eV, which is in good agreement with the activation energy calculated using Bube's equation (see Figure S2). The lower limit of trap density was estimated from the time integral of the TSC signal using

$$\int I_{\mathrm{TSC}} dt \leq e N_{\mathrm{t}} dA$$

where N_t is the trap density, e is the elementary charge, d is the thickness of the active layer, and A is the area of the device. After evaluating the peak P3 of the pristine device, the trap density came out to be ~ 2.3 x10^{15} cm^{-3}. In the case of thermally stressed solar cells for the duration of 300 and 400 hours, the additional peak is not much pronounced due to a comparatively low trap density, but it is quite dominating in the cell with 500 hours of thermal stress. Therefore, the trap energy corresponding to P4 was estimated for the samples with 500 hours of thermal stress and found to be ~ 0.414 eV. Whereas the lower limit of trap density, which was determined to be ~ 6.5 x10^{15} cm^{-3}, has the contribution from P3 as well as P4. The trap densities for all the devices contributed by the peak P3, and P4 are shown in Table 1. As the density of trapped carriers emitted during the heating process will undergo recombination prior to leaving the sample and possible incomplete filling of the trap states during illumination, our number gives a lower limit for the trap densities. The detrimental effect of these trap states in solar cells is due to the non-radiative recombination involving these states and thus reducing the *V*oc. This is in line with the *V*oc reduction with increasing thermal stress duration. It is to be noted that the density of the traps induced by thermal stress was found to increase consistently with thermal stress duration while the pristine trap peak (P3) initially increased and then returned to its previous value. This observation is reflected in the variation in total trap densities from pristine to 500 h thermally treated cell (as shown in Table 1), which increases till 400 h then slightly decreases till 500 h.

Table 1. The calculated activation energies and trap densities for all the devices

Thermal stress time (h)	E_t3 (eV)	E_t4 (eV)	N_t (cm^{-3})
0	0.459	--	2.3 x10^{15}

300	0.459	0.414	3.1 x10^{15}
400	0.459	0.414	7.8 x10^{15}
500	--	0.414	6.5x10^{15}

The x-ray diffraction (XRD) patterns show the presence of PbI_2 (corresponds to peak at ~ 12.8º) in $MAPbI_3$, which increases with thermal treatment time (Figure 4).[35] The PbI_2 itself in $MAPbI_3$ bulk does not act as trap states as the conduction and valence band edges of PbI_2 are out of the band gap of $MAPbI_3$ but would rather act as a scattering center for the carriers.[35,54]

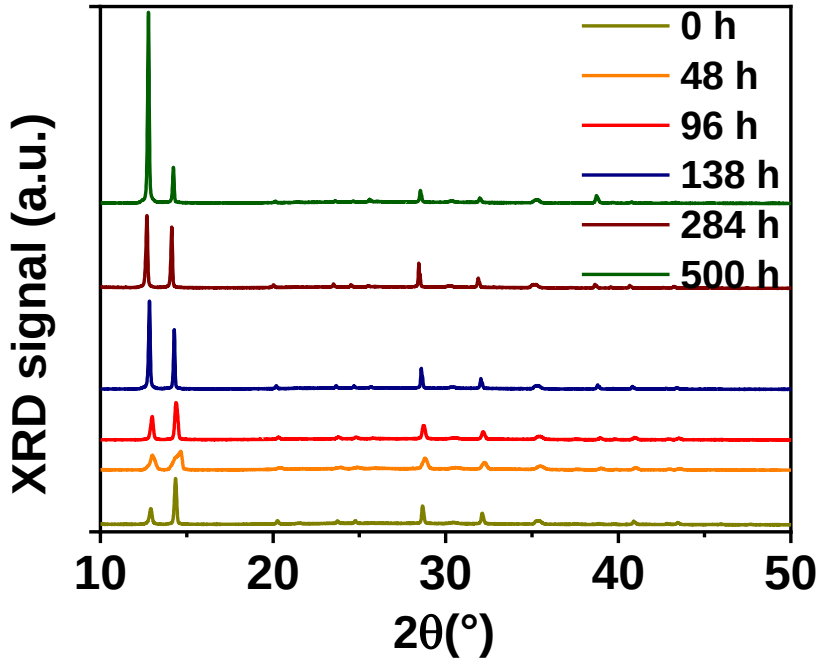

Figure 4. XRD profiles of $MAPbI_3$ films after different thermal stress times (at 85 ºC) from pristine to 500 hours.

The thermal decomposition of the $MAPbI_3$ structure takes place through the statistical formation of molecular defects with a non-ionic character (HI and MAI vacancies). This is invoked as a possible reason for the origin of the deep trap states.[55] Depending on the activation energy of the traps, there could be several possibilities of the

origin of the traps. The activation energy of 0.44 eV for iodine vacancies in $MAPbI_3$ was observed through First-Principles calculation as well as using temperature-dependent conductivity.[56,57] Moreover, the deep defect level due to the lead interstitials (Pbi) has been reported to be ~ 0.5 eV.[58] Although the activation energies of the above-mentioned traps are comparable to the obtained activation energy of the traps, there is no direct explanation for their enhancement on increasing the thermal stress duration. Recently we have shown the thermal decomposition of $MAPbI_3$ into PbI_2 and MAI leaving from the perovskite layer. The leaving of MAI from $MAPbI_3$ layer could create MAI vacancies.[49] As the XRD results show, thermal decomposition of $MAPbI_3$ increases with thermal stress duration, creating more MAI vacancies. Our observations (enhancement in trap states with thermal stress duration) are in line with this assumption, and MAI vacancies are the most probable source of traps. In addition, the peak intensity P4 was found to increase with the thermal stress duration from 300 h to 500 h in almost the same manner as the reduction in P3. Since P3 was present in the pristine perovskite, thermal degradation into PbI_2 leads to the reduction in the bulk of $MAPbI_3$, which could be the possible reason for the reduction in the traps related to P3, which also shows the correlation between P3 and P4.

Overall, the long-term thermal stress at elevated temperature leads to the formation of deep trap states which is related to the thermal decomposition of $MAPbI_3$ perovskite. The enhancement in trap density with thermal duration follows the same trend as the presence of PbI_2 phase, which was revealed by XRD technique. The obtained deep traps could be the major source of non-radiative recombination, which was reflected in the reduction of open-circuit voltage with the thermal stress time. Our finding, the effect of long-term thermal stress at elevated temperature in terms of trap states and thermal decomposition of perovskite, will contribute in understanding the hidden science behind the thermal instability of perovskite solar cells.

In conclusion, we investigated the effect of thermal stress on the performances of $MAPbI_3$ based PSCs by varying the thermal stress duration up to 500 h prior to the HTL deposition. We used the TSC technique to investigate the trap states in thermally stressed $MAPbI_3$ solar cells. Three TSC peaks were observed in pristine cells. The low temperature peak was attributed to the transport layer materials, which was confirmed by performing TSC measurement on devices without transport layers. The TSC peak at ~ 170 K was attributed to the phase transition of the $MAPbI_3$ crystal from orthorhombic to tetragonal, while the third peak at ~ 225 K was assigned to the trap

distribution in perovskite. The effect of thermal stress was revealed by the emergence of an additional trap peak at ~ 205 K, which increased with thermal stress time. The activation energy of the deep trap states arising due to the thermal stress was estimated to be ~ 0.414 eV with the trap density ~ 10^{16} cm^{-3}. A correlation between thermal stress duration and trap formation was established, which was in line with the *V*oc reduction trend. The thermal decomposition of $MAPbI_3$ was observed with PbI_2 in the XRD patterns, possibly taking place through the formation of MAI vacancies resulting in the deep trap states. Our findings indicate that the thermal degradation is closely related to the trap formation in $MAPbI_3$, which provides guidance for developing perovskite solar cells with reduced traps and high thermal stability.

Experimental methods

The electron transport layer (ETL) was processed by spin coating colloidal solution of SnO_2 in water in the ambient atmosphere on prestructured ITO substrates (Lumtec) followed by subsequent annealing at 250 °C for 30 minutes. A solution containing PbI_2 and methylammonium iodide in DMF:DMSO solvent mixture with 4:1 ratio was spin coated on ETL coated ITO substrates. Subsequently, the substrates are annealed for 45 minutes at 100 °C. After the thermal stress test, HTL solution consisting of spiro-OMeTAD, 4-tert-butylpyridine (TBP, Sigma-Aldrich), a Bis(trifluoromethane) sulfonimide lithium salt solution (in acetonitrile) in chlorobenzene solvent was spin coated on perovskite films. Afterward, the films were exposed to air with a controlled relative humidity of 23% for oxidization overnight. A 60 nm thick gold contact is thermally evaporated through a shadow mask resulting in an active device area of 10.5 mm^2. More details can be found elsewhere.[49]

For the x-ray diffraction (XRD) measurements, a Bruker D2Phaser system with Cu-Kα radiation (λ = 1.5405 Å) was applied to determine the crystallite structure of the perovskite layers with different annealing times.

TSC measurements were conducted in a closed cycle He cryostat using helium gas as the heat transfer medium. The atmosphere of the sample chamber was replaced with helium gas to make it inert. The possible traps were filled by illuminating a white LED array on the devices through an optical window for 5 min. After switching off the illumination, the device was kept in the dark for another 5 min to allow thermalization of the carriers. Then, the device was heated up to room temperature with a constant rate of 7K min^{-1}. The TSC signal was monitored

using a sub-femtoamp source meter (Keithley 6430) during the heating. No external voltage was applied to measure the current, and the built-in field was used to collect the de-trapped carriers.

Acknowledgments

We gratefully acknowledge financial support by the Federal Ministry for Research and Education (BMBF) through the Initiating and Networking Funding of the Helmholtz Association (HYIG of U.W.P. (VH-NG-1148)), the Helmholtz Energy Materials Foundry (HEMF); and the project PEROSEED (ZT-0024). The authors also gratefully acknowledge financial support by the Virtual Materials Design (Virt-Mat) initiative at KIT and the Karlsruhe School of Optics & Photonics (KSOP).

Supporting Information:

TSC spectra with two consecutive heat cycles, justification for using T^4 method to calculate activation energy of the traps and its comparison with Bube´s method and activation energy calculation with varying heating rate.

References:

(1) Kojima, A.; Teshima, K.; Shirai, Y.; Miyasaka, T. Organometal Halide Perovskites as Visible-Light Sensitizers for Photovoltaic Cells. *J. Am. Chem. Soc.* **2009**, *131* (17), 6050–6051.

(2) Lee, M. M.; Teuscher, J.; Miyasaka, T.; Murakami, T. N.; Henry J. Snaith. Efficient Hybrid Solar Cells Based on Meso-Superstructured Organometal Halide Perovskites. *Science* **2012**, *338* (6107), 643–647.

(3) National Renewable Energy Laboratory, Efficiency Chart (2021); www.nrel.gov/pv/cell-efficiency.html.

(4) Tian, J.; Wang, J.; Xue, Q.; Niu, T.; Yan, L.; Zhu, Z.; Li, N.; Brabec, C. J.; Yip, H. L.; Cao, Y. Composition Engineering of All-Inorganic Perovskite Film for Efficient and Operationally Stable Solar Cells. *Adv. Funct. Mater.* **2020**, *30* (28), 2001764.

(5) Wang, D.; Wu, C.; Luo, W.; Guo, X.; Qi, X.; Zhang, Y.; Zhang, Z.; Qu, B.; Xiao, L.; Chen, Z. Glass Rod-Sliding and Low Pressure Assisted Solution Processing Composition Engineering for High-Efficiency Perovskite Solar Cells. *Sol. Energy Mater. Sol. Cells* **2020**, *211*, 110532.

(6) Nie, W.; Tsai, H.; Asadpour, R.; Neukirch, A. J.; Gupta, G.; Crochet, J. J.; Chhowalla, M.; Tretiak, S.; Alam, M. A.; Wang, H. High-Efficiency Solution-Processed Perovskite Solar Cells with Millimeter-Scale Grains. *Science* **2015**, *347* (6221), 522–526.

(7) Ahn, N.; Son, D. Y.; Jang, I. H.; Kang, S. M.; Choi, M.; Park, N. G. Highly Reproducible Perovskite Solar Cells with Average Efficiency of 18.3% and Best Efficiency of 19.7% Fabricated via Lewis Base Adduct of Lead(II) Iodide. *J. Am. Chem. Soc.* **2015**, *137* (27), 8696–8699.

(8) Gao, L.; Li, X.; Liu, Y.; Fang, J.; Huang, S.; Spanopoulos, I.; Li, X.; Wang, Y.; Chen, L.; Yang, G.; Kanatzidis, M. G. Incorporated Guanidinium Expands the CH3NH3PbI3 Lattice and Enhances Photovoltaic Performance. *ACS Appl. Mater. Interfaces* **2020**, *12* (39), 43885–43891.

(9) Gharibzadeh, S.; Abdollahi Nejand, B.; Jakoby, M.; Abzieher, T.; Hauschild, D.; Moghadamzadeh, S.; Schwenzer, J. A.; Brenner, P.; Schmager, R.; Haghighirad, A. A.; Weinhardt, L.; Lemmer, U.; Richards, B. S.; Howard, I. A.; Paetzold, U. W. Record Open-Circuit Voltage Wide-Bandgap Perovskite Solar Cells Utilizing 2D/3D Perovskite Heterostructure. *Adv. Energy Mater.* **2019**, *9* (21), 1–10.

(10) Stolterfoht, M.; Caprioglio, P.; Wolff, C. M.; Márquez, J. A.; Nordmann, J.; Zhang, S.; Rothhardt, D.; Hörmann, U.; Amir, Y.; Redinger, A.; Kegelmann, L.; Zu, F.; Albrecht, S.; Koch, N.; Kirchartz, T.; Saliba, M.; Unold, T.; Neher, D. The Impact of Energy Alignment and Interfacial Recombination on the Internal and External Open-Circuit Voltage of Perovskite Solar Cells. *Energy Environ. Sci.* **2019**, *12* (9), 2778–2788.

(11) Park, N. G.; Zhu, K. Scalable Fabrication and Coating Methods for Perovskite Solar Cells and Solar Modules. *Nat. Rev. Mater.* **2020**, *5* (5), 333–350.

(12) Wu, M.; Haji Ladi, N.; Yi, Z.; Li, H.; Shen, Y.; Wang, M. Stability Issue of Perovskite Solar Cells under Real-World Operating Conditions. *Energy Technol.* **2020**, *8* (4), 1–12.

(13) Meng, L.; You, J.; Yang, Y. Addressing the Stability Issue of Perovskite Solar Cells for Commercial Applications. *Nature Communications*. **2018**, *9* (5265), 1–4.

(14) Huang, H. H.; Liu, Q. H.; Tsai, H.; Shrestha, S.; Su, L. Y.; Chen, P. T.; Chen, Y. T.; Yang, T. A.; Lu, H.; Chuang, C. H.; Lin, K. F.; Rwei, S. P.; Nie, W.; Wang, L. A Simple One-Step Method with Wide Processing Window for High-Quality Perovskite Mini-Module Fabrication. *Joule*. **2021**, *5* (4), 958–974.

(15) Luo, D.; Su, R.; Zhang, W.; Gong, Q.; Zhu, R. Minimizing Non-Radiative Recombination Losses in Perovskite Solar Cells. *Nature Reviews Materials*. **2020**, *5*, 44–60.

(16) Almora, O.; Baran, D.; Bazan, G. C.; Berger, C.; Cabrera, C. I.; Catchpole, K. R.; Erten-Ela, S.; Guo, F.; Hauch, J.; Ho-Baillie, A. W. Y.; Jacobsson, T. J.; Janssen, R. A. J.; Kirchartz, T.; Kopidakis, N.; Li, Y.; Loi, M. A.; Lunt, R. R.; Mathew, X.; McGehee, M. D.; Min, J.; Mitzi, D. B.; Nazeeruddin, M. K.; Nelson, J.; Nogueira, A. F.; Paetzold, U. W.; Park, N. G.; Rand, B. P.; Rau, U.; Snaith, H. J.; Unger, E.; Vaillant-Roca, L.; Yip, H. L.; Brabec, C. J. Device Performance of Emerging Photovoltaic Materials (Version 1). *Adv. Energy Mater.* **2021**, *11* (11), 2002774.

(17) Ball, J. M.; Petrozza, A. Defects in Perovskite-Halides and Their Effects in Solar Cells. *Nat. Energy* **2016**, *1* (11), 1–13.

(18) Stranks, S. D. Nonradiative Losses in Metal Halide Perovskites. *ACS Energy Lett.* **2017**, *2* (7), 1515–1525.

(19) Boyd, C. C.; Cheacharoen, R.; Leijtens, T.; McGehee, M. D. Understanding Degradation Mechanisms and Improving Stability of Perovskite Photovoltaics. *Chem. Rev.* **2019**, *119* (5), 3418–3451.

(20) Schwenzer, J. A.; Rakocevic, L.; Gehlhaar, R.; Abzieher, T.; Gharibzadeh, S.; Moghadamzadeh, S.; Quintilla, A.; Richards, B. S.; Lemmer, U.; Paetzold, U. W. Temperature Variation-Induced Performance Decline of Perovskite Solar Cells. *ACS Appl. Mater. Interfaces* **2018**, *10* (19), 16390–16399.

(21) Bastos, J. P.; Paetzold, U. W.; Gehlhaar, R.; Qiu, W.; Cheyns, D.; Surana, S.; Spampinato, V.; Aernouts, T.; Poortmans, J. Light-Induced Degradation of Perovskite Solar Cells: The Influence of 4-Tert-Butyl Pyridine and Gold. *Adv. Energy Mater.* **2018**, *8* (23), 1800554.

(22) Shi, D.; Adinolfi, V.; Comin, R.; Yuan, M.; Alarousu, E.; Buin, A.; Chen, Y.; Hoogland, S.; Rothenberger, A.; Katsiev, K.; Losovyj, Y.; Zhang, X.; Dowben, P. A.; Mohammed, O. F.; Sargent, E. H.; Bakr, O. M. Low Trap-State Density and Long Carrier Diffusion in Organolead Trihalide Perovskite Single Crystals. *Science* . **2015**, *347* (6221), 519–522.

(23) Kim, J.; Lee, S. H.; Lee, J. H.; Hong, K. H. The Role of Intrinsic Defects in Methylammonium Lead Iodide Perovskite. *J. Phys. Chem. Lett.* **2014**, *5* (8), 1312–1317.

(24) Agiorgousis, M. L.; Sun, Y. Y.; Zeng, H.; Zhang, S. Strong Covalency-Induced Recombination Centers in Perovskite Solar Cell Material CH3NH3PbI3. *J. Am. Chem. Soc.* **2014**, *136* (41), 14570–14575.

(25) Li, W.; Sun, Y. Y.; Li, L.; Zhou, Z.; Tang, J.; Prezhdo, O. V. Control of Charge Recombination in Perovskites by Oxidation State of Halide Vacancy. *J. Am. Chem. Soc.* **2018**, *140* (46), 15753–15763.

(26) Li, W.; Liu, J.; Bai, F. Q.; Zhang, H. X.; Prezhdo, O. V. Hole Trapping by Iodine Interstitial Defects Decreases Free Carrier Losses in Perovskite Solar Cells: A Time-Domain Ab Initio Study. *ACS Energy Lett.* **2017**, *2* (6), 1270–1278.

(27) Yin, W. J.; Shi, T.; Yan, Y. Unusual Defect Physics in CH3NH3PbI3 Perovskite Solar Cell Absorber. *Appl. Phys. Lett.* **2014**, *104* (6), 063903.

(28) Gao, Y.; Wu, Y.; Liu, Y.; Chen, C.; Bai, X.; Yang, L.; Shi, Z.; Yu, W. W.; Dai, Q.; Zhang, Y. Dual Functions of Crystallization Control and Defect Passivation Enabled by an Ionic Compensation Strategy for Stable and High-Efficient Perovskite Solar Cells. *ACS Appl. Mater. Interfaces* **2020**, *12* (3), 3631–3641.

(29) Ambrosio, F.; Mosconi, E.; Alasmari, A. A.; Alasmary, F. A. S.; Meggiolaro, D.; De Angelis, F.

Formation of Color Centers in Lead Iodide Perovskites: Self-Trapping and Defects in the Bulk and Surfaces. *Chem. Mater.* **2020**, *32* (16), 6916–6924.

(30) Zhang, L.; Liu, Y.; He, X.; Ye, H.; Leng, J.; Ren, X.; Jin, S.; Liu, S. Cd-Doped Triple-Cation Perovskite Thin Films with a 20 Ms Carrier Lifetime. *J. Phys. Chem. C* **2020**, *124* (40), 22011–22018.

(31) Buin, A.; Pietsch, P.; Xu, J.; Voznyy, O.; Ip, A. H.; Comin, R.; Sargent, E. H. Materials Processing Routes to Trap-Free Halide Perovskites. *Nano Lett.* **2014**, *14* (11), 6281–6286.

(32) Heo, S.; Seo, G.; Lee, Y.; Lee, D.; Seol, M.; Lee, J.; Park, J. B.; Kim, K.; Yun, D. J.; Kim, Y. S.; Shin, J. K.; Ahn, T. K.; Nazeeruddin, M. K. Deep Level Trapped Defect Analysis in CH3NH3PbI3 Perovskite Solar Cells by Deep Level Transient Spectroscopy. *Energy Environ. Sci.* **2017**, *10* (5), 1128–1133.

(33) Baumann, A.; Väth, S.; Rieder, P.; Heiber, M. C.; Tvingstedt, K.; Dyakonov, V. Identification of Trap States in Perovskite Solar Cells. *J. Phys. Chem. Lett.* **2015**, *6* (12), 2350–2354.

(34) Shrestha, N.; Song, Z.; Chen, C.; Bastola, E.; Wang, X.; Yan, Y.; Ellingson, R. J. Charge Compensating Defects in Methylammonium Lead Iodide Perovskite Suppressed by Formamidinium Inclusion. *J. Phys. Chem. Lett.* **2020**, *11* (1), 121–128.

(35) Qin, C.; Matsushima, T.; Fujihara, T.; Potscavage, W. J.; Adachi, C. Degradation Mechanisms of Solution-Processed Planar Perovskite Solar Cells: Thermally Stimulated Current Measurement for Analysis of Carrier Traps. *Adv. Mater.* **2016**, *28* (3), 466–471.

(36) Aristidou, N.; Eames, C.; Sanchez-Molina, I.; Bu, X.; Kosco, J.; Saiful Islam, M.; Haque, S. A. Fast Oxygen Diffusion and Iodide Defects Mediate Oxygen-Induced Degradation of Perovskite Solar Cells. *Nat. Commun.* **2017**, *8*, 15218.

(37) Gordillo, G.; Otálora, C. A.; Reinoso, M. A. Trap Center Study in Hybrid Organic-Inorganic Perovskite Using Thermally Stimulated Current (TSC) Analysis. *J. Appl. Phys.* **2017**, *122* (7), 075304.

(38) Lanzetta, L.; Aristidou, N.; Haque, S. A. Stability of Lead and Tin Halide Perovskites: The Link between

Defects and Degradation. *J. Phys. Chem. Lett*. **2020**, *11* (2), 574–585.

(39) Wu, J.; Shi, J.; Li, Y.; Li, H.; Wu, H.; Luo, Y.; Li, D.; Meng, Q. Quantifying the Interface Defect for the Stability Origin of Perovskite Solar Cells. *Adv. Energy Mater*. **2019**, *9* (37), 1901352.

(40) Bastos, J. P.; Uytterhoeven, G.; Qiu, W.; Paetzold, U. W.; Cheyns, D.; Surana, S.; Rivas, J.; Jaysankar, M.; Song, W.; Aernouts, T.; Poortmans, J.; Gehlhaar, R. Model for the Prediction of the Lifetime and Energy Yield of Methyl Ammonium Lead Iodide Perovskite Solar Cells at Elevated Temperatures. *ACS Appl. Mater. Interfaces* **2019**, *11* (18), 16517–16526.

(41) Conings, B.; Drijkoningen, J.; Gauquelin, N.; Babayigit, A.; D'Haen, J.; D'Olieslaeger, L.; Ethirajan, A.; Verbeeck, J.; Manca, J.; Mosconi, E.; De Angelis, F.; Boyen, H. G. Intrinsic Thermal Instability of Methylammonium Lead Trihalide Perovskite. *Adv. Energy Mater.* **2015**, *5* (15), 1–8.

(42) Yu, X.; Qin, Y.; Peng, Q. Probe Decomposition of Methylammonium Lead Iodide Perovskite in N2 and O2 by in Situ Infrared Spectroscopy. *J. Phys. Chem. A* **2017**, *121* (6), 1169–1174.

(43) Schwenzer, J. A.; Rakocevic, L.; Abzieher, T.; Rueda-Delgado, Di.; Moghadamzadeh, S.; Gharibzadeh, S.; Hossain, I. M.; Gehlhaar, R.; Richards, B. S.; Lemmer, U.; Paetzold, U. W. Toward Stable Perovskite Solar Cell Architectures: Robustness against Temperature Variations of Real-World Conditions. *IEEE J. Photovoltaics* **2020**, *10* (3), 777–784.

(44) Haering, R. R.; Adams, E. N. Theory and Application of Thermally Stimulated Currents in Photoconductors. *Phys. Rev.* **1960**, *117* (2), 451–454.

(45) Schafferhans, J.; Deibel, C.; Dyakonov, V. Electronic Trap States in Methanofullerenes. *Adv. Energy Mater*. **2011**, *1* (4), 655–660.

(46) Moghadamzadeh, S.; Hossain, I. M.; Jakoby, M.; Abdollahi Nejand, B.; Rueda-Delgado, D.; Schwenzer, J. A.; Gharibzadeh, S.; Abzieher, T.; Khan, M. R.; Haghighirad, A. A.; Howard, I. A.; Richards, B. S.; Lemmer, U.; Paetzold, U. W. Spontaneous Enhancement of the Stable Power Conversion Efficiency in

Perovskite Solar Cells. *J. Mater. Chem. A* **2020**, *8* (2), 670–682.

(47) Hu, Y.; Hutter, E. M.; Rieder, P.; Grill, I.; Hanisch, J.; Aygüler, M. F.; Hufnagel, A. G.; Handloser, M.; Bein, T.; Hartschuh, A.; Tvingstedt, K.; Dyakonov, V.; Baumann, A.; Savenije, T. J.; Petrus, M. L.; Docampo, P. Understanding the Role of Cesium and Rubidium Additives in Perovskite Solar Cells: Trap States, Charge Transport, and Recombination. *Adv. Energy Mater.* **2018**, *8* (16), 1–11.

(48) Farooq, A.; Khan, M. R.; Abzieher, T.; Voigt, A.; Lupascu, D. C.; Lemmer, U.; Richards, B. S.; Paetzold, U. W. Photodegradation of Triple-Cation Perovskite Solar Cells: The Role of Spectrum and Bias Conditions. *ACS Appl. Energy Mater.* **2021**, *4* (4), 3083–3092.

(49) Schwenzer, J. A.; Hellmann, T.; Nejand, B. A.; Hu, H.; Abzieher, T.; Schackmar, F.; Hossain, I. M.; Fassl, P.; Mayer, T.; Jaegermann, W.; Lemmer, U.; Paetzold, U. W. Thermal Stability and Cation Composition of Hybrid Organic-Inorganic Perovskites. *ACS Appl. Mater. Interfaces* **2021**, *13* (13), 15292–15304..

(50) Duong, T.; Pham, H.; Kho, T. C.; Phang, P.; Fong, K. C.; Yan, D.; Yin, Y.; Peng, J.; Mahmud, M. A.; Gharibzadeh, S.; Nejand, B. A.; Hossain, I. M.; Khan, M. R.; Mozaffari, N.; Wu, Y. L.; Shen, H.; Zheng, J.; Mai, H.; Liang, W.; Samundsett, C.; Stocks, M.; McIntosh, K.; Andersson, G. G.; Lemmer, U.; Richards, B. S.; Paetzold, U. W.; Ho-Ballie, A.; Liu, Y.; Macdonald, D.; Blakers, A.; Wong-Leung, J.; White, T.; Weber, K.; Catchpole, K. High Efficiency Perovskite-Silicon Tandem Solar Cells: Effect of Surface Coating versus Bulk Incorporation of 2D Perovskite. *Adv. Energy Mater.* **2020**, *10* (9), 1903553.

(51) Leoncini, M.; Giannuzzi, R.; Giuri, A.; Colella, S.; Listorti, A.; Maiorano, V.; Rizzo, A.; Gigli, G.; Gambino, S. Electronic Transport, Ionic Activation Energy and Trapping Phenomena in a Polymer-Hybrid Halide Perovskite Composite. *J. Sci. Adv. Mater. Devices* **2021**, *6* (4), 543–550.

(52) Fang, Z.; Shan, L.; Schlesinger, T. E.; Milnes, A. G. Study of Defects in LEC-Grown Undoped SI-GaAs by Thermally Stimulated Current Spectroscopy. *Mater. Sci. Eng. B* **1990**, *5* (3), 397–408.

(53) Bube, R. H. Opto-Electronic Properties of Mercuric Iodide. *Phys. Rev.* **1957**, *106* (4), 703–717.

(54) Chen, Q.; Zhou, H.; Song, T. Bin; Luo, S.; Hong, Z.; Duan, H. S.; Dou, L.; Liu, Y.; Yang, Y. Controllable Self-Induced Passivation of Hybrid Lead Iodide Perovskites toward High Performance Solar Cells. *Nano Lett.* **2014**, *14* (7), 4158–4163.

(55) Deretzis, I.; Alberti, A.; Pellegrino, G.; Smecca, E.; Giannazzo, F.; Sakai, N.; Miyasaka, T.; La Magna, A. Atomistic Origins of CH3NH3PbI3 Degradation to PbI2 in Vacuum. *Appl. Phys. Lett.* **2015**, *106* (13), 131904.

(56) Haruyama, J.; Sodeyama, K.; Han, L.; Tateyama, Y. First-Principles Study of Ion Diffusion in Perovskite Solar Cell Sensitizers. *J. Am. Chem. Soc.* **2015**, *137* (32), 10048–10051.

(57) Yang, T. Y.; Gregori, G.; Pellet, N.; Grätzel, M.; Maier, J. The Significance of Ion Conduction in a Hybrid Organic-Inorganic Lead-Iodide-Based Perovskite Photosensitizer. *Angew. Chemie - Int. Ed.* **2015**, *54* (27), 7905–7910.

(58) Yin, W. J.; Shi, T.; Yan, Y. Unique Properties of Halide Perovskites as Possible Origins of the Superior Solar Cell Performance. *Adv. Mater.* **2014**, *26* (27), 4653–4658.